Integration of DInSAR time series with GNSS data for volcanic eruption early warning applications

Authors: Brianna Corsa (Brianna.Corsa@Colorado.edu); Magali Barba-Sevilla; Kristy Tiampo; Charles Meertens

University of Colorado
CIRES and Department of Geological Sciences

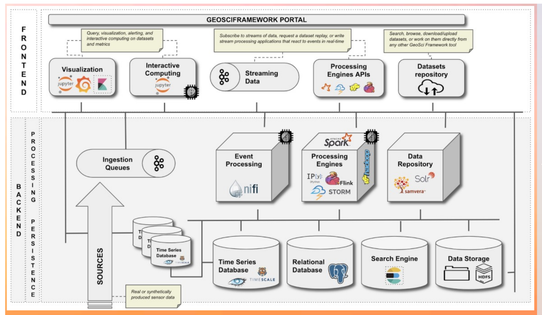

Figure 1: GeoSCIFramework Project Architecture. At the top, "Frontend" depicts the different user-facing components that the GSF provides: from visualization and interactive computing tools to streaming data, static datasets, and even direct access to advanced analytics frameworks. At bottom, "Backend" shows the different components that take care of the heavy lifting: ingesting, curating and consolidating data, computational processing, and dataset management.

Project Background:

What is GSF?

- The collaborative GeoSCIFramework (GSF) project aims to improve volcano, earthquake, and tsunami early warning applications

How?

- Apply big data analytics and machine learning methods to large streams of real-time data from a mix of seismic, geodetic-related sensors, and differential interferometric synthetic aperture radar (DInSAR) satellite imagery.

Why?

- It will provide researchers with a suite of datasets and a means to detect, monitor, and analyze geophysical activity over a region of interest.

Focus Here?

- Preparation of DInSAR + GNSS integrated dataset for volcano modeling and streaming through machine learning algorithms

Methodology:

Part I: Automated processing of DInSAR imagery over Hawaii from Nov. 2015- April 2021 (SLC → Interferogram)

- GMTSAR source code (now using ISCE2 Stack Processor)
- Orbital, topographic, and atmospheric corrections, must be applied to isolate the deformation signal.
- 35 Allowed Days between image pairs: 250 descending SLC images → 671 interferograms

Part II: DInSAR time series generation

- Additional atmospheric (GACOS) and topographic corrections
- Applies SBAS/NSBAS inversion methods
- GIAnT (now using MintPY) time series software

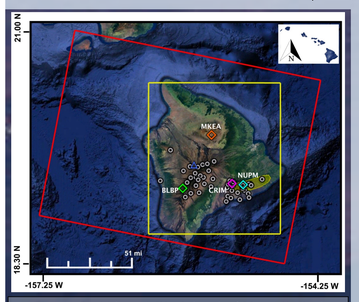

Figure 2: (Above) Big Island of Hawaii. Red outline shows SAR scene extent, Path 87 Frame 526. Yellow box shows cropped outline of each interferogram. Grey circles and colored diamonds indicate GNSS station locations. We take a closer look at the time series over the purple diamond represents CRIM station. Blue triangle shows the location of the Mauna Loa volcano summit, and the yellow polygon indicates where the East Rift Zone is located.

Figure 3: (Below) We expand on the DInSAR + GNSS velocity integration method developed by Samsonov 2006, which uses a Bayesian statistical model in conjunction with Markov random field (MRF) theory to combine datasets with varying spatio-temporal extents.

The energy function is as follows:

$$U(\boldsymbol{b}/\boldsymbol{a}) = \sum_{i=1}^{N} \frac{(b_i - a_i)^2}{2\sigma_i^2} \quad (1)$$

where $U\left(\frac{a}{b}\right)$ is the likelihood energy, b is the observation with uncertainty, σ, a is the unknown parameter, and N is the number of observations, or pixels within the acquisition. The resulting adaptation of Equation S1 to our geodetic displacement datasets is:

$$U(d^{LOS}, d_x^{GPS}, d_y^{GPS}, d_z^{GPS}/d_x, d_y, d_z) = \sum_{i=1}^{N} C^{LOS}\,(d^{LOS} - S_x^{LOS} d_x - S_y^{LOS} d_y - S_z^{LOS} d_z)^2 + C_x^{GPS}(d_x^{GPS} - d_x)^2 + C_y^{GPS}(d_y^{GPS} - d_y)^2 + C_z^{GPS}(d_z^{GPS} - d_z)^2 \quad (2)$$

with coefficients

$$C^{LOS} = \frac{1}{2(\sigma^{LOS})^2}, \quad C_x^{GPS} = \frac{1}{2(\sigma_x^{GPS})^2}, \quad C_y^{GPS} = \frac{1}{2(\sigma_y^{GPS})^2}, \quad C_z^{GPS} = \frac{1}{2(\sigma_z^{GPS})^2} \quad (3)$$

where σ is the standard deviation for the measurements, d^{LOS} is the cumulative LOS displacement, $[S_x^{LOS}, S_y^{LOS}, S_z^{LOS}]$ are the unit vectors pointing from the ground to the satellite, and $[d_x^{GPS}, d_y^{GPS}, d_z^{GPS}]$ are the 3D displacements from the kriging interpolated GNSS data.

Part III: Integration of DInSAR and GNSS data from 48 overlapping stations in Hawaii

- GNSS is known for high precision in the horizontal directions (east and north) but vertical motions have larger uncertainty.
- DInSAR sensors are most sensitive to vertical displacements and can improve ground velocity estimates in the up direction

- Displacements aligned to fixed Pacific plate to minimize linear trends of tectonic motion
- Ordinary kriging algorithm with exponential model to generate variograms
- Outputs three cumulative displacement maps (east, north, and up) with same discretization/geocoding as DInSAR output

- Integration of DInSAR + GNSS data is based off Samsonov, 2006 and involves a Bayesian statistical model with Markov Random Field Theory and outputs with 100-m resolution

- Over large areas, the code produced 3D high-resolution cumulative displacement maps and the corresponding uncertainties for each individual date or time-step of the series.
- At a single point where DInSAR and GNSS overlap, can pull integrated time series

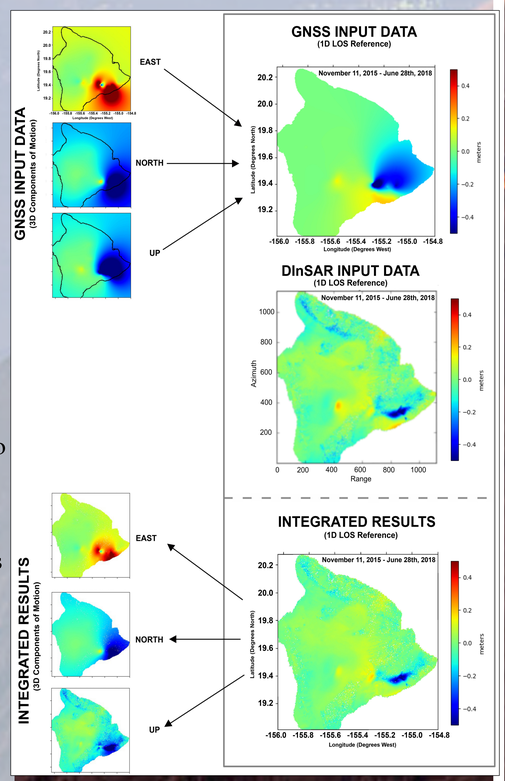

Figure 4: Diagram of our project methodology and integration between DInSAR and GNSS data. First, GNSS variograms are generated using data from 48 stations in Hawaii. Transformed to the same discretion as the DInSAR time series, the two are combined to create a fused dataset with more constrained uncertainties. The fused dataset may be delivered to researchers over a large area in the form of a map, or at a single pixel location as a plotted time series.

Results

Figure 5 and 6 show results from the 3D cumulative displacement maps provide new information regarding the pre-, during-, and post-eruption phases of the Hawaiian volcanic system at unprecedented spatial scales and revealed surface effects from magma movement and seismic activity leading to two different types of eruptions. The results from integrating the GNSS data with the DInSAR data showed a more constrained uplift pattern than the DInSAR or GNSS results alone.

Figure 5: (Left) Comparison of (a) the final time-step of the integrated time series converted to LOS with (b) the final cumulative LOS DInSAR scene and (c) the final cumulative GNSS interpolated map, also converted to LOS.

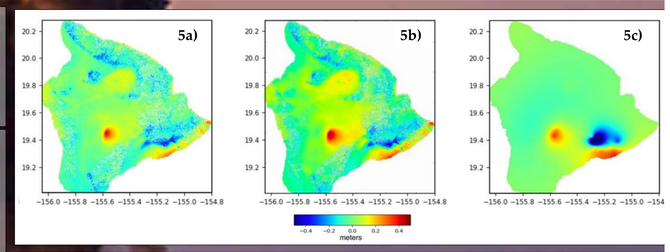

Figure 6: (Right) a) Final, cumulative uncertainty distribution for the 3D integrated displacement maps (November 2015-April 2021). b) Total uncertainty results associated with figure a. Uncertainties are combined from errors associated with the raw DInSAR and GNSS time series data and additional error introduced from applying the kriging algorithm to interpolate the GNSS data and produce variograms.

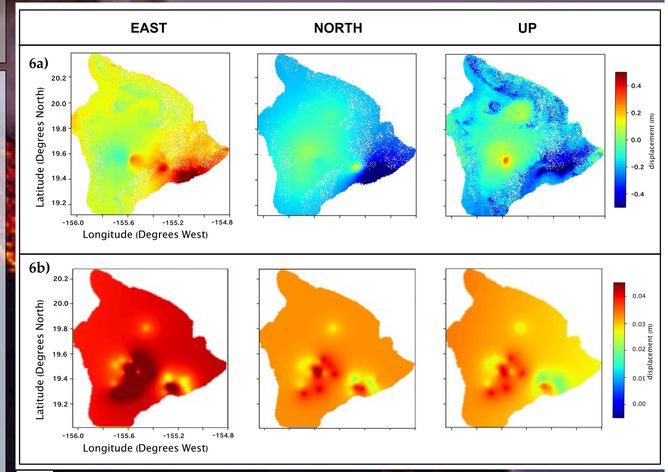

Uncertainty Analysis:

- As a result of the interpolation method, uncertainties associated with the integrated, cumulative 3D displacement maps are greater than the uncertainties calculated at a single pixel .

- Maximum uncertainties in the east, north, and up directions are 7.07 cm, 5.82 cm, and 5.72 cm, respectively.

Figures 7 and 8 show results from the plotted time series at a single pixel, where CRIM GNSS station and the DInSAR time series overlap (see subset plot in Figure 7a.

Figure 7: Integrated results compared to original, raw GNSS time series in the (a) east-, (b) north-, and (c) up-components of motion at the CRIM GNSS station (19.395°N, –155.274°W). Plotted time series allow us to thoroughly describe ground motion at a single pixel.

Figure 8: Integrated uncertainty for the plotted time series at the overlapping pixel location for CRIM GNSS station in the a) horizontal and b) vertical directions.

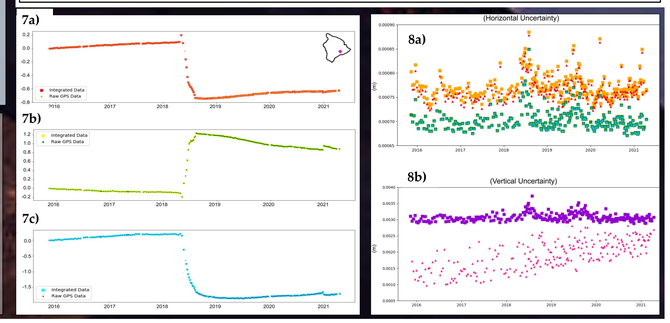

Future Work:

Link to publication and references therewithin:

Volcanic source modeling using both DInSAR and fused results

- Spherical Mogi *(1958)*
- Non-linear spherical *(Yang et al., 1988)*
- Sill-like *(Fialko et al., 2001)*
- Dyke/Horizontal tensile dislocation *(Okada, 1985)*

Generate synthetic training dataset

- Using the volcanic source parameter results from above and methods developed by (Lee et al., 2016), we will develop an artificial data set that will be used for training the machine learning algorithm.

Apply machine learning on datasets and test with real data

- Hawaii has 3 eruptions captured in time series sequence. After training the MLA, we will apply it to each eruption separately and test whether it is able to forecast the other eruptive events